MEMORANDUM REPORT NO. 1298
AUGUST 1960

# A STUDY OF JETS

# FROM

# SCALED CONICAL SHAPED CHARGE LINERS

R. DiPersio
J. Simon
T. H. Martin

## BALLISTIC RESEARCH LABORATORIES

# ABERDEEN PROVING GROUND, MARYLAND

# BALLISTIC RESEARCH LABORATORIES

## MEMORANDUM REPORT NO. 1298

### AUGUST 1960

## A STUDY OF JETS FROM SCALED CONICAL SHAPED CHARGE LINERS

R. DiPersio

J. Simon

T. H. Martin

Terminal Ballistic Laboratory

ABERDEEN PROVING GROUND, MARYLAND

# TABLE OF CONTENTS

BALLISTIC RESEARCH LABORATORIES

MEMORANDUM REPORT NO. 1298

RDiPersio/JSimon/THMartin/ebh
Aberdeen Proving Ground, Maryland
August 1960

A STUDY OF JETS FROM SCALED CONICAL SHAPED CHARGE LINERS

ABSTRACT

Triple flash radiographs of jets from three scaled shaped charges containing copper cones with apex angle of $42^\circ$ are analyzed. The performance of jet particles was determined by numbering particles as shown on time sequenced radiographs, and obtaining their velocity. Penetration characteristics of jets in terms of the action of these discrete particles are described.

# I. INTRODUCTION

X-ray photography for observing the jets produced by lined shaped charges has become an important research tool to explain jet behavior. The obstructing cloud of smoke and flame which detracts from ordinary photographic processes, does not affect flash-radiographs which produce clear, sharp outlines of the jet material with exposuretimes of the order of 0.1 microsecond.

A triple flash field radiographic system has been in operation at the Ballistic Research Laboratories since February 1952, and was reported in 1953.[1] Each X-ray tube is positioned at an angle of 120 degrees with respect to its immediate neighbor. The film holder, receiving normal radiation from its corresponding X-ray tube, is also at an angle of 120 degrees with its adjoining neighbor. Each film holder contains three X-ray films with dimensions 4" x 17", laid end to end for a total length of 51". The round is detonated above a blast protection plate. The jet passes through a hole in this armor shielding plate, and travels parallel to the length of the three film cassettes. The X-ray tubes are triggered at pre-determined and set time intervals after charge initiation.

For a short time interval after collapse of the shaped charge liner walls, the material from the inside of the liner forms a continuous axial jet. The gradient in velocity between the front and rear of the jet causes the jet to increase in length with time. This produces stress on the solid jet material which causes it to neck, and then break up into many individual particles. With all other conditions equal, the time of initial jet breakup depends upon the physical properties of the metal used to form the liner. Jets formed by ductile metal liners remain in the continuous state for a longer time than those obtained from less ductile ones. For example, a steel jet breaks up sooner than a copper jet.

This report will deal exclusively with the properties of jets
from conical copper liners having an apex angle of 42 degrees. Three
charges, scaled in all linear dimensions, have been studied to determine
the effect of charge size upon jet flight and jet penetration characteristics.
The methods used are an extension of those of Breidenbach.[2]

## II. JET CHARACTERISTICS IN FLIGHT

### A. Charge Description

The charges used were dimensionally proportional to the numbers 2;
3; 4; and they will henceforth be referred to as charge numbers 2, 3,
and 4. A diagram of the copper cone, and steel casing enclosing it, are
given in Figures 1 and 2. The dimensions for all charges are given below
the figures. Composition B explosive surrounded the liner and was initiated
by an M-36 initiator and tetryl booster.

### B. Velocity Gradient of Jet

Triple flash radiographs of the jets from charge sizes 2, 3, and
4 are shown in Figure 3. The time in microseconds after initiation is
noted in each case. These times were selected to be long enough to detect
the particle structure of the jet. The earliest view of the number 4
charge jet is absent due to malfunction of the X-ray tube. In any case,
the earliest flash is not as useful as the latter two, because jet breakup
is not complete at this early time. Corresponding jet particles in the
second and third flash of each jet are distinguishable and have been
numbered on the X-ray photograph consecutively from tip to rear. Measure-
ments on the individual particles were made directly on the original radio-
graphs. The relative positions of the X-ray tube, jet, and film were
arranged to produce only negligible magnification on the film. However,
some error was introduced when the three 4" x 17" film panels were glued
together to show the complete jet. These panels were enclosed in film
holders when exposed and their butting ends produced a gap of up to 1/2
cm. between adjacent films.

The measurements made on the radiographs are indicated in Figure 3. The distance from the jet tip to the front of each particle is designated by $\ell$. The measurement from the top of the X-ray film to the front of a particle is denoted by Y. The velocity of each jet particle is given by $\dfrac{Y_3 - Y_2}{t_3 - t_2}$ where the subscripts indicate which of the three sequenced flashes is used. The data for a number 2 charge size are given in Table No. 1.

Effective penetration by a jet ceases when the particle velocity drops slightly below 0.2 cm/microsecond[3]. Measurements of jet particles have been made only as far as this lower velocity limit. The length of jet from the tip of the leading particle to the rear of the last effective particle is denoted by L. The ratio $\ell/L$, for each particle at the second and third radiographic times are given in the table and the average taken.

A plot of the jet particle velocity as a function of its relative position from the jet tip $\left(\dfrac{(\ell)}{L}\right)$ for the three scaled charges is given in Figure 4. The gradient in velocity shown in this manner is independent of time. The points for each charge are represented by the same straight line. The apparent periodic drop of the points below this line was caused by the error introduced by the joining seams of the film panel as mentioned previously. The reverse gradient exhibited by the first one or two particles, however, appears to be real.

C. <u>Jet Velocity Vs. Position on Liner</u>

By firing shaped charges with radioactive tracer material deposited on the inner cone surface, into mild steel targets, the correspondence between particle position in the jet and its original position in the liner can be obtained by radioactive tracer techniques. The details of this analysis are given in reference 3. The final result is a curve of $\dfrac{\ell}{L}$ as a function of $\dfrac{x}{h}$ where x is the distance from the inside cone apex to a particular circumferential ring element on the inside liner

7

# TABLE 1

## Measurements of Jet Particles for No. 2 Charge

$t_2 = 187.4 \mu sec.$    $t_3 = 212.5 \mu sec.$    $L_2 = 100.3$ cm    $L_3 = 113.9$ cm

$$V_j = \frac{Y_3 - Y_2}{t_3 - t_2}$$

| Jet Particle Number | $\ell_2$ (cm) | $\ell_3$ (cm) | $Y_2$ (cm) | $Y_3$ (cm) | (mm/μsec) | $\frac{\ell_2}{L_2}$ | $\frac{\ell_3}{L_3}$ | av. $\frac{\ell}{L}$ | $\frac{x}{h}$ |
|---|---|---|---|---|---|---|---|---|---|
| 1 | 0 | 0 | 110.5 | 128.6 | 7.61 | 0 | 0 | 0 | .50 |
| 2 | 1.5 | 1.2 | 109.0 | 127.4 | 7.73 | .015 | .010 | .013 | .52 |
| 3 | 3.6 | 3.2 | 106.9 | 125.4 | 7.77 | .036 | .028 | .032 | .55 |
| 4 | 6.3 | 6.4 | 104.2 | 122.2 | 7.56 | .063 | .056 | .060 | .58 |
| 5 | 9.3 | 9.7 | 101.2 | 118.9 | 7.44 | .093 | .085 | .089 | .61 |
| 6 | 10.7 | 11.2 | 99.8 | 117.4 | 7.40 | .107 | .098 | .103 | .62 |
| 7 | 12.8 | 13.6 | 97.7 | 115.0 | 7.27 | .128 | .119 | .124 | .64 |
| 8 | 13.7 | 14.6 | 96.8 | 114.0 | 7.23 | .137 | .128 | .133 | .65 |
| 9 | 15.9 | 17.0 | 94.6 | 111.6 | 7.14 | .159 | .149 | .154 | .66 |
| 10 | 16.8 | 18.0 | 93.7 | 110.6 | 7.10 | .167 | .158 | .163 | .67 |
| 11 | 17.9 | 19.2 | 92.6 | 109.4 | 7.06 | .178 | .169 | .174 | .68 |
| 12 | 20.3 | 22.0 | 90.2 | 106.6 | 6.89 | .202 | .193 | .198 | .70 |
| 13 | 23.1 | 25.2 | 87.4 | 103.4 | 6.72 | .230 | .221 | .226 | .71 |
| 14 | 25.6 | 28.7 | 84.9 | 99.9 | 6.30 | .255 | .252 | .254 | .73 |
| 15 | 28.0 | 31.4 | 82.5 | 97.2 | 6.18 | .279 | .276 | .278 | .74 |

8

TABLE 1 (Continued)

$$V_j = \frac{Y_3 - Y_2}{t_3 - t_2}$$

| Jet Particle Number | $\ell_2$ (cm) | $\ell_3$ (cm) | $Y_2$ (cm) | $Y_3$ (cm) | (mm/μsec) | $\frac{\ell_2}{L_2}$ | $\frac{\ell_3}{L_3}$ | av. $\frac{\ell}{L}$ | $\frac{x}{h}$ |
|---|---|---|---|---|---|---|---|---|---|
| 16 | 29.7 | 33.3 | 80.8 | 95.3 | 6.09 | .296 | .292 | .294 | .75 |
| 17 | 31.8 | 35.6 | 78.7 | 93.0 | 6.01 | .317 | .313 | .315 | .76 |
| 18 | 34.2 | 38.4 | 76.3 | 90.2 | 5.84 | .341 | .337 | .339 | .77 |
| 19 | 39.8 | 44.2 | 70.7 | 84.4 | 5.76 | .397 | .388 | .393 | .79 |
| 20 | 41.0 | 45.7 | 69.5 | 82.9 | 5.63 | .409 | .401 | .405 | .80 |
| 21 | 43.5 | 48.7 | 67.0 | 79.9 | 5.42 | .434 | .428 | .431 | .81 |
| 22 | 45.1 | 50.4 | 65.4 | 78.2 | 5.38 | .450 | .442 | .446 | .81 |
| 23 | 47.2 | 52.7 | 63.3 | 75.9 | 5.29 | .471 | .463 | .467 | .82 |
| 24 | 49.5 | 55.3 | 61.0 | 73.3 | 5.17 | .494 | .486 | .490 | .82 |
| 25 | 50.4 | 56.5 | 60.1 | 72.1 | 5.04 | .502 | .496 | .499 | .83 |
| 26 | 52.7 | 59.1 | 57.8 | 69.5 | 4.92 | .525 | .519 | .522 | .83 |
| 27 | 54.5 | 61.2 | 56.0 | 67.4 | 4.79 | .543 | .537 | .540 | .84 |
| 28 | 58.1 | 65.2 | 52.4 | 63.4 | 4.62 | .579 | .572 | .576 | .84 |
| 29 | 60.3 | 67.8 | 50.2 | 60.8 | 4.45 | .601 | .595 | .598 | .85 |
| 30 | 63.0 | 70.8 | 47.5 | 57.8 | 4.33 | .628 | .622 | .625 | .85 |
| 31 | 65.1 | 73.4 | 45.4 | 55.2 | 4.12 | .649 | .644 | .647 | .85 |
| 32 | 67.4 | 76.0 | 43.1 | 52.6 | 3.99 | .672 | .667 | .670 | .86 |

TABLE 1 (Continued)

$$V_j = \frac{Y_3 - Y_2}{t_3 - t_2}$$

| Jet Particle Number | $\ell_2$ (cm) | $\ell_3$ (cm) | $Y_2$ (cm) | $Y_3$ (cm) | (mm/μsec) | $\frac{\ell_2}{L_2}$ | $\frac{\ell_3}{L_3}$ | av. $\frac{\ell}{L}$ | $\frac{x}{h}$ |
|---|---|---|---|---|---|---|---|---|---|
| 33 | 68.2 | 77.7 | 42.3 | 50.9 | 3.61 | .680 | .682 | .681 | .86 |
| 34 | 70.6 | 80.4 | 39.9 | 48.2 | 3.49 | .704 | .706 | .705 | .86 |
| 35 | 72.5 | 82.7 | 38.0 | 45.9 | 3.32 | .723 | .726 | .725 | .86 |
| 36 | 74.9 | 85.4 | 35.6 | 43.2 | 3.19 | .747 | .750 | .749 | .87 |
| 37 | 76.2 | 86.6 | 34.3 | 42.0 | 3.24 | .760 | .760 | .760 | .87 |
| 38 | 77.5 | 88.1 | 33.0 | 40.5 | 3.15 | .773 | .773 | .773 | .87 |
| 39 | 78.7 | 89.5 | 31.8 | 39.1 | 3.07 | .785 | .786 | .786 | .88 |
| 40 | 80.8 | 91.9 | 29.7 | 36.7 | 2.94 | .806 | .807 | .807 | .88 |
| 41 | 82.8 | 94.2 | 27.7 | 34.4 | 2.82 | .826 | .827 | .827 | .88 |
| 42 | 83.6 | 95.2 | 26.9 | 33.4 | 2.73 | .833 | .836 | .835 | .89 |
| 43 | 86.9 | 99.0 | 23.6 | 29.6 | 2.52 | .866 | .869 | .868 | .90 |
| 44 | 87.9 | 100.1 | 22.6 | 28.5 | 2.48 | .876 | .879 | .878 | .90 |
| 45 | 89.4 | 101.8 | 21.1 | 26.8 | 2.39 | .891 | .894 | .893 | .90 |
| 46 | 90.9 | 103.5 | 19.6 | 25.1 | 2.31 | .906 | .909 | .908 | .90 |
| 47 | 91.5 | 104.2 | 19.0 | 24.4 | 2.27 | .912 | .915 | .914 | .91 |
| 48 | 93.3 | 106.2 | 17.2 | 22.4 | 2.18 | .930 | .932 | .931 | .92 |
| 49 | 94.7 | 107.7 | 15.8 | 20.9 | 2.14 | .944 | .946 | .945 | .92 |
| 50 | 96.8 | 110.4 | 13.7 | 18.2 | 1.89 | .965 | .969 | .967 | .93 |
| 51 | 99.3 | 113.0 | 11.2 | 15.6 | 1.85 | .990 | .992 | .991 | .94 |

10

surface (measured along the cone axis), and h is the total cone height. It is found that only negligible jet material originates in that half of the cone including the apex. Values of $\frac{x}{h}$ given in Table I were obtained from this curve. A plot of data for jet particle velocity versus relative position on the cone given for all three charges in Figure 5, indicates that a single smooth curve represents the functional relationship for all three scaled charges.

D.  Jet Particle Number vs Position on Liner

A plot of the jet particle number from the front versus the relative position of its origin on the cone liner is shown in Figure 6. Again, a single smooth curve suffices for the data of all three scaled charges. It is seen that the number of particles per unit cone height increases rapidly with distance from the apex until near the cone base where the flange inhibits jet formation.

E.  Jet Particle Measurements

The length of each particle at the second and third radiographic times, and, the space length between particles, were measured. A summary of these data are given in Table 2.

The radiographs were taken at about the same time for each charge. At these unscaled times, the jet dispersion process is most advanced for the smallest charge. The jet from Charge No. 2 appears to have completed its break up at times $t_2$ and $t_3$. The jet from charge size No. 3 contains distinct particles near the rear at time $t_3$ which were still joined together at time $t_2$. The point of eventual breakup is evident in the joined particles, so that individual numbers were assigned to the segments seen on the photograph. The jet from charge No. 4 contains large particles near the rear which would doubtless subdivide at a time later than $t_3$. The most obvious division points have been used as a basis of numbering in this region.

TABLE 2

Lengths of Jet Particles and Spaces Between Particles

| Time (μ sec) | Charge No. 2 | | Charge No. 3 | | Charge No. 4 | |
|---|---|---|---|---|---|---|
| | $t_2 = 187.4$ | $t_3 = 212.5$ | $t_2 = 186.9$ | $t_3 = 211.2$ | $t_2 = 189.0$ | $t_3 = 214.0$ |
| No. of particles | 51 | 51 | 51 | 51 | 49 | 49 |
| Sum of particle lengths (cm) | 47.4 | 48.7 | 74.9 | 76.1 | 88.4 | 94.6 |
| Sum of space lengths (cm) | 53.8 | 66.0 | 24.0 | 38.0 | 7.6 | 17.6 |

12

Despite the lack of full breakup shown in Jet No. 4, it appears that all scaled jets eventually break up into approximately the same number of particles. Table 2 shows that these particles increase very little in length with increased time. Almost all of the jet length increase with time, after break up, is accounted for by the increased space between adjacent particles.

Although the individual jet particles are quite irregular in shape, a mean diameter was measured for each and an average obtained for each jet. The volume of jet material was then computed as being that of a cylinder with this average diameter and observed total length. The jet mass was estimated by assuming a jet density equal to the copper liner density, 8.9 gms/cc. These data are summarized in Table 3.

TABLE 3

Jet Mass Determination

| Charge Size | 2 | 3 | 4 |
|---|---|---|---|
| Sum of Particle Lengths (cm) | 47.4 | 74.9 | 88.4 |
| Average Particle Diameter (cm) | 0.20 | 0.37 | 0.45 |
| Jet Mass (grams) | 12.8 | 71.1 | 125.0 |
| Mass of Jet $\div$ Mass of Liner | .155 | .256 | .188 |

Although the measurements are necessarily crude, the results indicate that the jet particle lengths and diameters scale in approximately the same ratio as the charge sizes. About 20 percent of the liner material goes into the jet formation. This percentage does not hold constant over all of the cone height.

Figure 6 shows that the number of jet particles formed in the
zone from $\frac{x}{h}$ = 0.8 to 0.9 is approximately half the total number
formed. This is a much greater number than can be accounted for
by the larger diameter of the zone near the base. Also the particle
sizes are larger nearer the base. The percentage of jet material
contributed by the half of the cone including the apex is considered
negligible.

## III. JET PENETRATION CHARACTERISTICS

### A. Penetration - Time Measurements

The scaled charges were fired into a target of 6" x 6" x 1" stacked
mild steel target plates at a standoff of three cone diameters. The
time that the jet pierced each inch of the target was recorded on an
oscilloscope by means of electrical contacts sandwiched between plates.
The data pertaining to the number 4 charge are given in Table 4. The
cumulative penetrations and times have been normalized by division by
the cone diameter. The penetration-time data for all three charges are
plotted in this normalized fashion in Figure 7. The closely grouped
plotted points justify a single smooth curve to represent all of the
charges regardless of size.

### B. Penetration Velocity

The average jet penetration velocity through each 1" of target
plate is obtained in Table 4 by division by the penetration time per
plate. Figure 8 shows these data for the three charges as a function
of the normalized time after initial penetration. The data in this case
are more scattered than heretofore, but a single smooth curve is again
indicated as representative of the phenomena.

### C. Jet Velocity

It is possible to calculate the jet tip velocity at each inch of
target depth by making use of the fact that each jet particle travels
with an essentially constant velocity. The jet can be assumed to originate

14

## TABLE 4

### Penetration Characteristics of No. 4 Charge

Standoff-Three Cone Diameters; Target = 6" x 6" x 1" mild steel plates

| P Target Thickness (inches) | t Time After Initial Penetration ($\mu$ sec) | Penetration Time Per Plate ($\mu$ sec) | U Penetration Velocity (cm/$\mu$ sec) | $\dfrac{P}{D}$ Cone Dia. | $\dfrac{t}{D} = (\dfrac{\mu sec}{cm})$ | $V_j$ = Jet Velocity (cm/$\mu$sec) |
|---|---|---|---|---|---|---|
| 1 | 6.7 | 6.7 | 0.379 | 0.26 | 0.70 | 0.755 |
| 2 | 12.3 | 5.6 | .454 | .53 | 1.28 | .728 |
| 3 | 20.2 | 7.9 | .322 | .79 | 2.11 | .680 |
| 4 | 30.4 | 10.2 | .249 | 1.06 | 3.17 | .626 |
| 5 | 38.8 | 8.4 | .302 | 1.31 | 4.04 | .594 |
| 6 | 48.1 | 9.3 | .273 | 1.59 | 5.02 | .563 |
| 7 | 58.1 | 10.0 | .254 | 1.85 | 6.05 | .537 |
| 8 | 68.7 | 10.6 | .240 | 2.22 | 7.15 | .517 |
| 9 | 79.3 | 10.6 | .240 | 2.38 | 8.25 | .487 |
| 10 | 89.7 | 10.4 | .244 | 2.65 | 9.35 | .469 |
| 11 | 104.1 | 14.4 | .176 | 2.91 | 10.85 | .441 |
| 12 | 115.8 | 11.7 | .217 | 3.18 | 12.06 | .425 |
| 13 | 128.8 | 13.0 | .195 | 3.44 | 13.42 | .408 |
| 14 | 142.8 | 14.0 | .181 | 3.71 | 14.89 | .392 |
| 15 | 160.8 | 18.0 | .141 | 3.97 | 16.76 | .370 |

TABLE 4 (Continued)

| P Target Thickness (inches) | t Time After Initial Penetration ($\mu$ sec) | Penetration Time Per Plate ($\mu$ sec) | U Penetration Velocity (cm/$\mu$ sec) | $\dfrac{P}{D}$ Cone Dia. | $\dfrac{t}{D} = (\dfrac{\mu sec}{cm})$ | Jet $V_j$ = Velocity (cm/$\mu$sec) |
|---|---|---|---|---|---|---|
| 16 | 174.9 | 14.1 | .180 | 4.23 | 18.23 | .358 |
| 17 | 194.2 | 19.3 | .132 | 4.50 | 20.24 | .340 |
| 18 | 216.1 | 21.9 | .116 | 4.77 | 22.50 | .322 |
| 19 | 238.1 | 22.7 | .112 | 5.03 | 24.90 | .305 |
| 20 | 270.8 | 32.0 | .079 | 5.30 | 28.20 | .283 |
| 21 | 300.3 | 29.5 | .086 | 5.56 | 31.20 | .267 |
| 22 | 411.8 | 111.5 | .022 | 5.82 | 42.80 | .208 |

Total penetration = 22.5" = 5.95 cone diameters

at a single point on its axis just forward of the cone apex.[3,4]
The distance from this point to the surface of any of the plates
in the target divided by the time of flight to this point gives the
jet particle velocity just starting its penetration. The equation
used is :

$$V_j = \frac{A + P}{B + t} \; ,$$  (1)

where A is the distance from the point origin of the jet to the top
of the target, and B is the time the front jet particle reaches the
target. B is obtained from the known jet tip velocity and the distance
A. P is depth of penetration at time t.

The equation of $V_j$ is the same for each of the scaled charges if each
term is divided by the cone diameter, D. For the three cone diameter
standoff used, the resultant equation is:

$$V_j = \frac{4.13 + \frac{P}{D}}{5.12 + \frac{t}{D}}$$  (2)

The calculated jet velocities are given in Table 4 and plotted in Figure 8.

D. Jet Penetration Theory

From the hydrodynamic theory of jet formation[5], the jet penetration
velocity and the corresponding jet tip velocity are related by the equation:

$$\frac{U}{V-U} = \sqrt{\frac{\lambda \rho_j}{\rho_t}}$$  (3)

Where:  U = penetration velocity
        V = jet velocity
        $\rho_t$ = target density
        $\rho_j$ = jet density
        $\lambda$ = numerical factor

This equation does not consider the effects of target strength, which
could become important for the slower moving particles near rear of jet.[6]
The linear jet density (mass per unit length, $\rho_j$) decreases with time due
to the jet elongation. The manner of variation of the product, $\lambda \rho_j$, may
be determined by equation 3.

TABLE 5

Calculation of Jet "Breakup" Factor

| $\dfrac{t}{D}$ $\mu$ sec/cm | $V$ cm/$\mu$ sec | $U$ cm/$\mu$ sec | $\dfrac{U}{V-U} = \sqrt{\dfrac{\lambda \rho_j}{\rho_t}}$ |
|---|---|---|---|
| 0 | 0.808 | 0.400 | 0.980 |
| 1 | .726 | .370 | 1.039 |
| 2 | .672 | .343 | 1.043 |
| 3 | .628 | .322 | 1.052 |
| 4 | .591 | .301 | 1.038 |
| 5 | .558 | .283 | 1.029 |
| 6 | .532 | .267 | 1.008 |
| 7 | .508 | .252 | 0.984 |
| 8 | .486 | .240 | .976 |
| 9 | .467 | .227 | .946 |
| 10 | .450 | .216 | .923 |
| 11 | .434 | .205 | .895 |
| 12 | .420 | .196 | .875 |
| 13 | .405 | .185 | .841 |
| 14 | .395 | .179 | .829 |
| 15 | .383 | .172 | .815 |
| 16 | .372 | .165 | .797 |
| 17 | .362 | .159 | .783 |
| 18 | .353 | .152 | .756 |
| 19 | .345 | .147 | .742 |
| 20 | .338 | .141 | .716 |
| 21 | .330 | .135 | .692 |
| 22 | .323 | .130 | .674 |
| 23 | .316 | .124 | .646 |
| 24 | .310 | .118 | .615 |
| 25 | .303 | .113 | .595 |

18

## TABLE 5 (Continued)

| $\dfrac{t}{D}$ $\mu$ sec/cm | $V$ cm/$\mu$ sec | $U$ cm/$\mu$ sec | $\dfrac{U}{V-U} = \sqrt{\dfrac{\lambda \rho_j}{\rho_t}}$ |
|---|---|---|---|
| 26 | .297 | .106 | .555 |
| 27 | .290 | .101 | .534 |
| 28 | .282 | .098 | .533 |
| 29 | .277 | .093 | .505 |
| 30 | .270 | .090 | .500 |
| 31 | .265 | .085 | .472 |
| 33 | .255 | .078 | .441 |
| 35 | .244 | .070 | .402 |
| 38 | .230 | .057 | .330 |
| 40 | .222 | .051 | .298 |
| 45 | .210 | .039 | .228 |

Table 5 was obtained by reading corresponding values of U and V from Figure 8. The "breakup" factor $\sqrt{\dfrac{\lambda \rho_j}{\rho_t}}$ , was then calculated from equation 3. A plot of the "breakup" factor is given as a function of time after initial penetration in Figure 9.

At an early time, before breakup occurs, the factor $\sqrt{\dfrac{\lambda \rho_j}{\rho_t}}$ should be simply equal to the square root of the ratio of the jet to target densities. For the copper jet and steel target used here, this factor would equal 1.07. This is nearly the maximum value calculated after the start of penetration. At later times, the "breakup" factor decreases monotonically.

## IV. CONCLUSIONS

(1) The radiographic techniques used in this work have provided data for the establishment of tentative scaling laws for a homologous family of shaped charges.

(2) The data of this report provides confirmatory evidence for previously reported concepts of jet behavior utilizing different experimental methods, and verified the following conclusions:

a. The jet velocity gradient for most purposes can be satisfactorily approximated by a constant at any given time except for the first few jet particles. Its value varies inversely with the charge size at the same time, and inversely with time for the same charge. This property has been determined previously by means of streak camera records and electronic recording taken mainly by the Carnegie Institute of Technology.

b. Approximately 20 per cent of the cone mass results in jet material, for the charges described. This measurement has been determined with more accuracy by slug recovery experiments[6].

c. Scaled shaped charges produce scaled penetration depths at scaled standoff distances. The penetration velocities, jet velocities, and relative penetration depths are the same at scaled times during the penetration process. The method used in this report for penetration study was the same as that used by the Carnegie Institute of Technology.

(3) In addition to the above, two conclusions relating to jet behavior can be drawn which cannot be obtained by any other method than radiographic observation:

a. Jets from scaled conical liners in scaled charges produce approximately the same number of particles after breakup is completed. The number of particles produced by the charges used in the present study was in the neighborhood of 50. The average particle length scales directly as the charge size. Also the average particle diameter varies directly as the charge size so that the average particle volume and mass varies as the cube of the charge size.

b. The increase in jet length, after breakup, is accomplished almost wholly by separation between jet particles. Although jet material stretches and decreases its diameter early in the formation process, this characteristic stops when complete breakup is obtained. Each particle then travels with a single characteristic velocity with no appreciable stretching occurring.

R. DIPERSIO

J. SIMON

T. H. MARTIN

21

## V. REFERENCES

*1. Kronman, S., Simon, J., and et al, "A Triple Flash Field Radiograph System For Studying Jets From Large Shaped Charges", BRLM 659, March 1953.

*2. Breidenbach, H. I., "The Evolution of Jets From Cavity Charges As Shown By Flash Radiographs", BRL 808, April 1952.

*3. DiPersio, R., and Simon, J., "An Emperical Approach to the Design of a Spin-Compensating Shaped Charge Liner", BRLM 1251, February 1960.

4. Allison, F. E., and Bryan, G. M., "Cratering By a Train of Hypervelocity Fragments", Proceedings of the Second Hypervelocity Impact Effects Symposium, Vol. 1, December 1957.

5. Birkhoff, G., McDougal, D. P., Pugh, E. M., Taylor, G., "Explosives with Lined Cavities", Journal of Applied Physics, Vol. 19, No. 6, pp 563-582, June 1948.

6. Eichelberger, R. J., "Re-examination of the Theories of Jet Formation and Target Penetration by Lined Cavity Charges", Carnegie Institute of Technology, Contract No. DA-36-ORD-394, June 1954: or Eichelberger, R. J., "Experimental Test of the Theory of Penetration by Metallic Jets", Journal of Applied Physics, Vol. 27, No. 1, pp 63-68, January 1956.

---

*Denotes a security classification
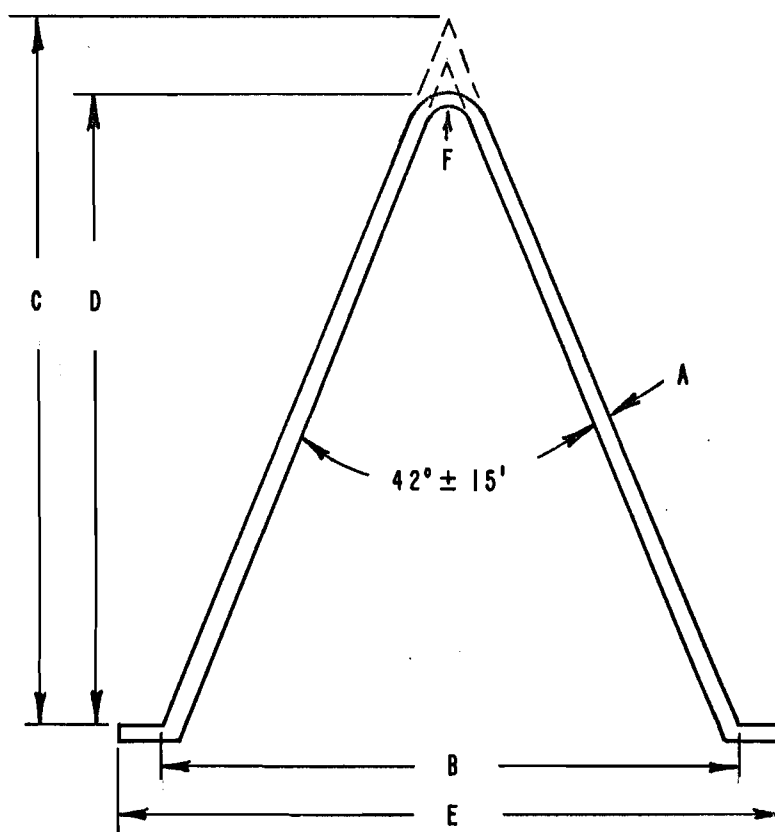
| DIMENSIONS | | SCALE SIZE NO. | | |
|---|---|---|---|---|
| | | 2 | 3 | 4 |
| A | NOMINAL WALL THICKNESS ⊥ WALL(IN.) | .070 | 0.105 | 0.140 |
| B | CONE DIAMETER (INCHES) | 1.890 | 2.835 | 3.780 |
| C | THEORETICAL ALTITUDE (INCHES) | 2.4618 | 3.6927 | 4.9236 |
| D | GEOMETRICAL HEIGHT (INCHES) | 2.238 | 3.357 | 4.476 |
| E | FLANGE DIAMETER (INCHES) | 2.050 | 3.075 | 4.100 |
| F | INSIDE RADIUS (INCHES) | .0625 | .093 | 0.125 |
| | MEASURED CONE MASS (GMS.) | 82.53 | 278.8 | 662.9 |

Fig. 1.  Dimensions of the BRL scaled copper liners.

CASING                                    TETRYL PELLET
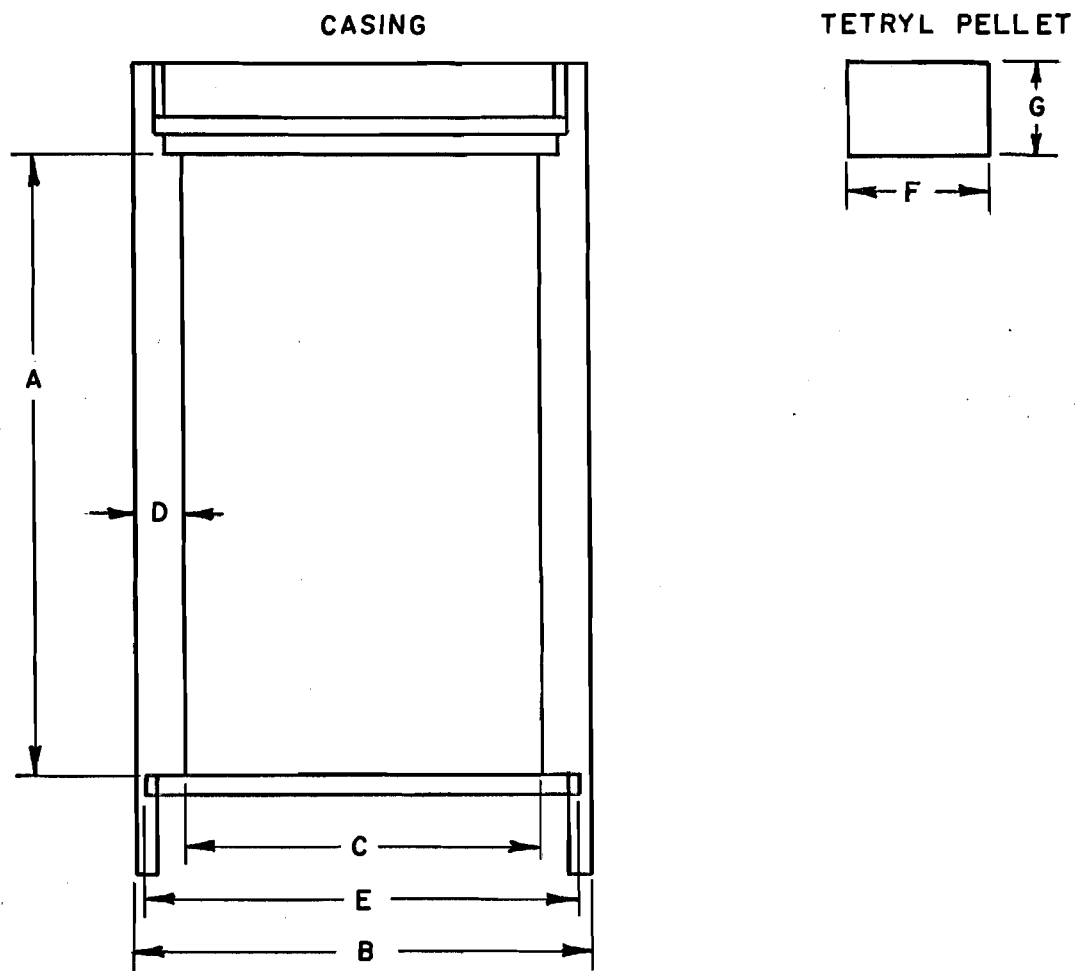


| | SCALE SIZE NO. | | |
|---|---|---|---|
| | 2 | 3 | 4 |
| **CASINGS** | | | |
| A - LENGTH (INCHES) | 3.271 | 4.894 | 6.525 |
| B - O. D. (INCHES) | 2.366 | 3.545 | 4.726 |
| C - I. D. (INCHES) | 1.892 | 2.837 | 3.782 |
| D - WALL THICKNESS (IN.) | 0.237 | 0.354 | 0.472 |
| E - FLANGE REGISTER | 2.051 | 3.076 | 4.101 |
| **TETRYL PELLETS** | | | |
| F - DIAMETER (INCHES) | 0.683 | 1.042 | 1.378 |
| G - LENGTH (INCHES) | 0.455 | 0.683 | 0.912 |

Fig. 2.  Scaled Dimensions for casings and tetryl pellets.
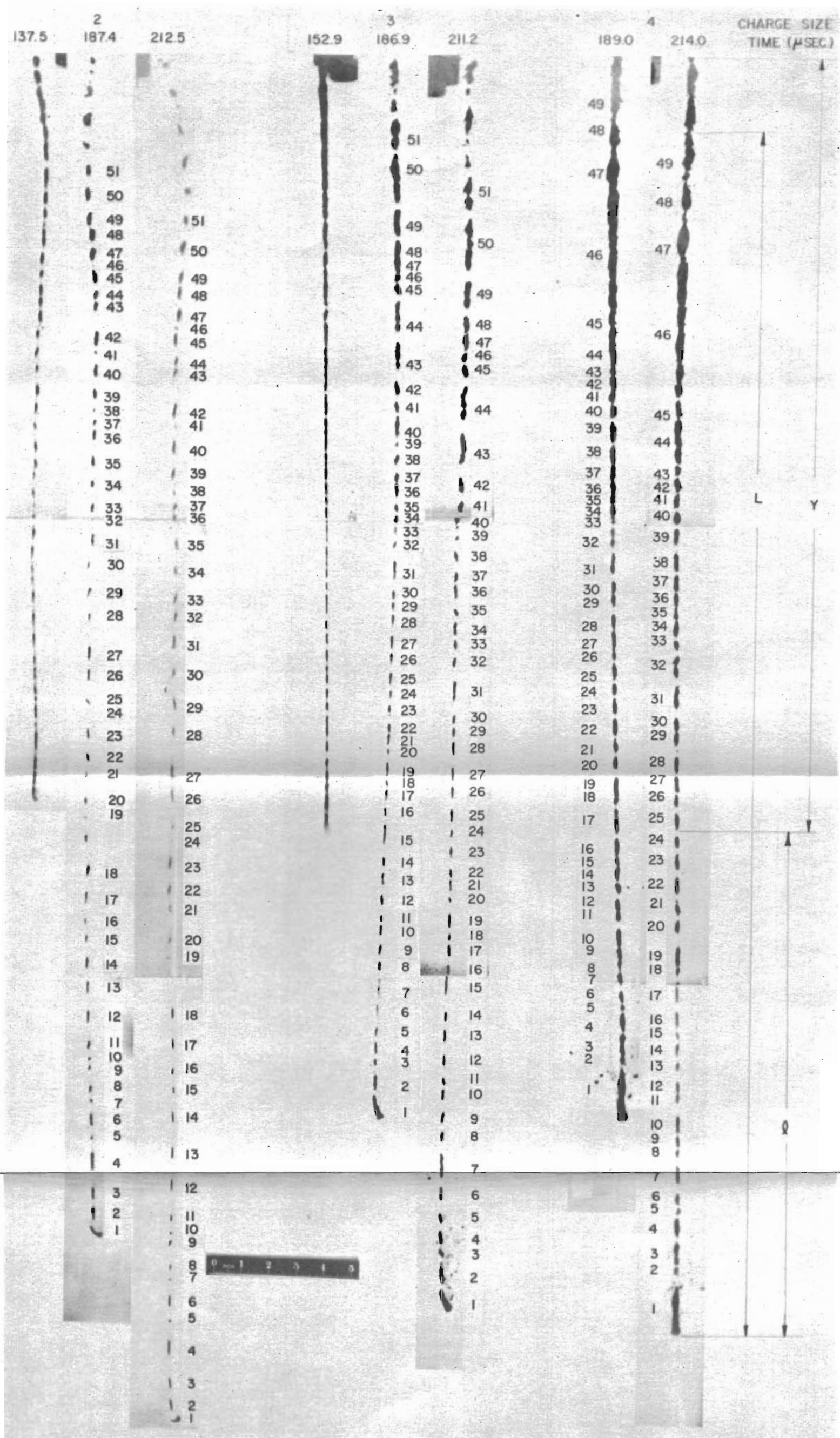
Fig. 3. Triple flash radiographs of jets from scaled charges.
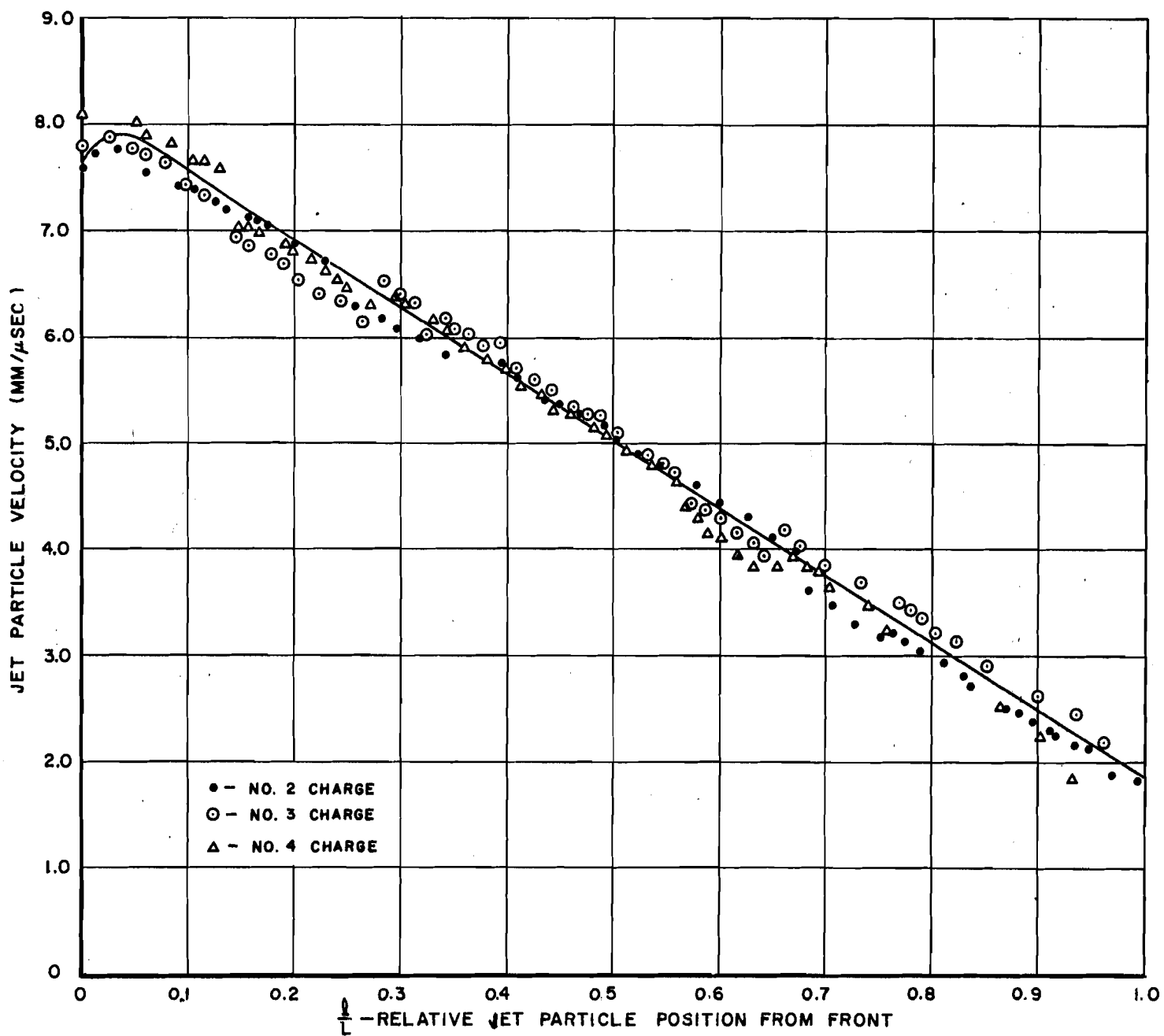
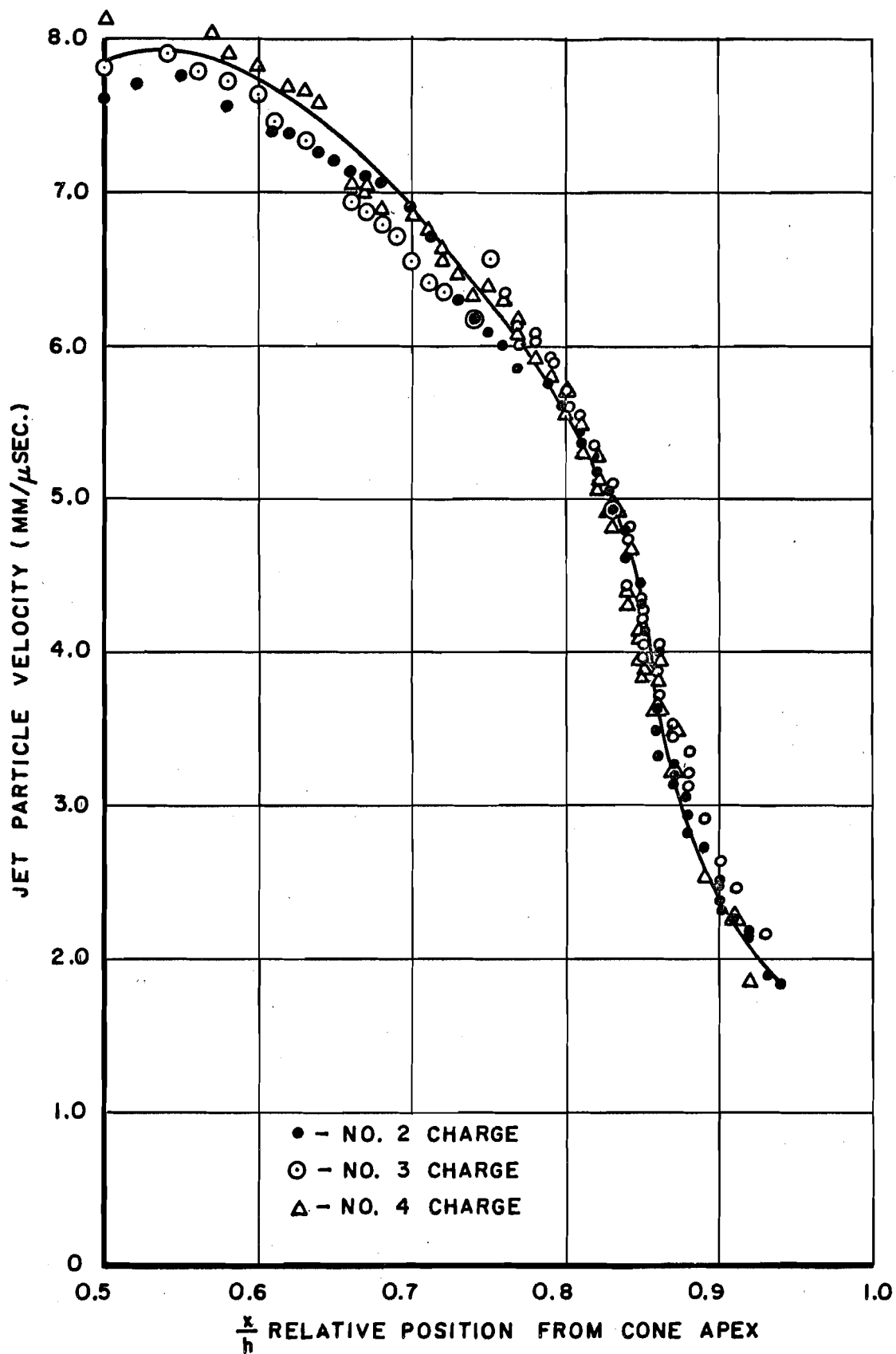Fig. 4. Velocity gradient of jets for three scaled charges.

27

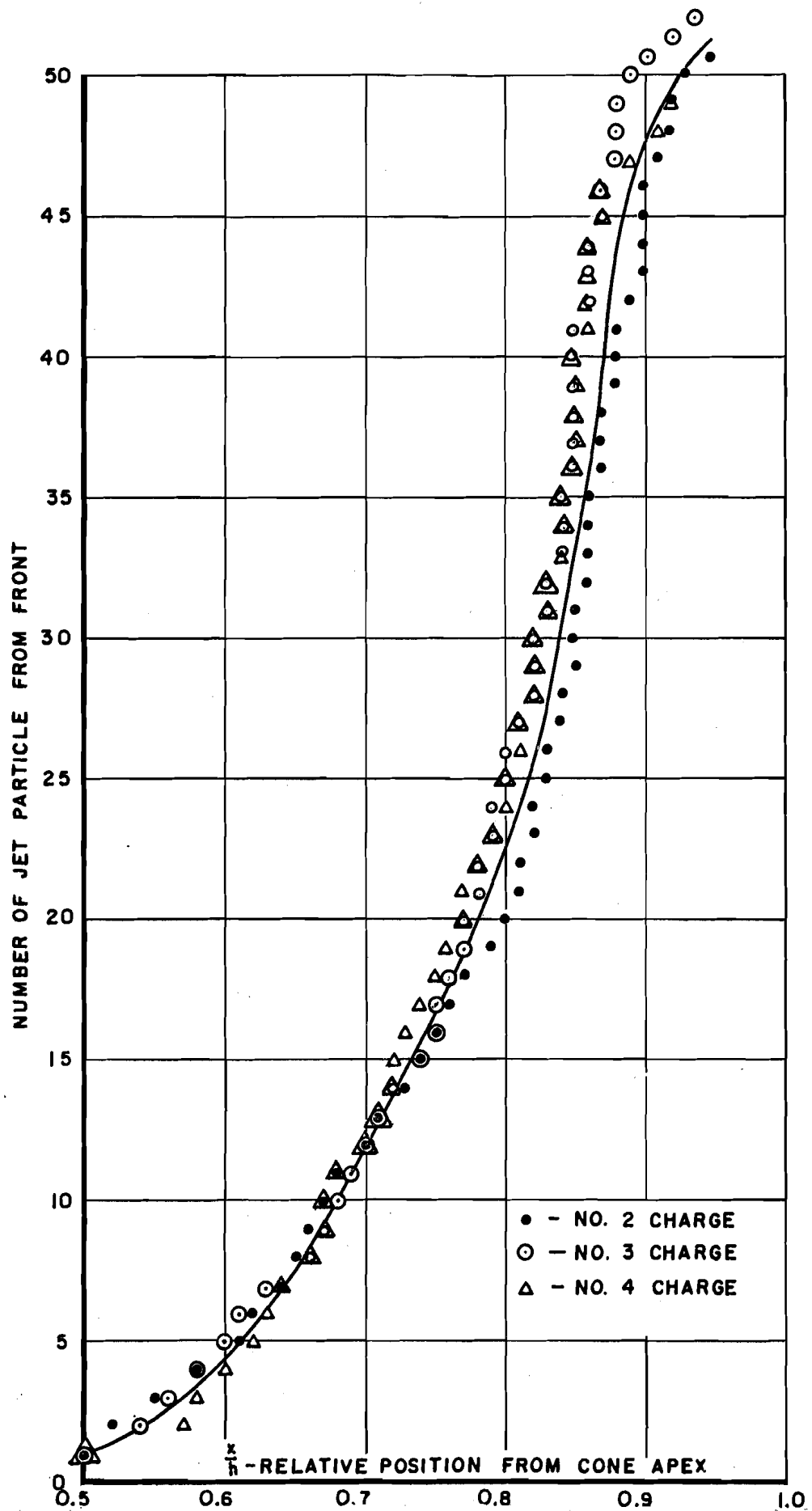Fig. 5. Jet particle velocity vs. original position on cone liner.

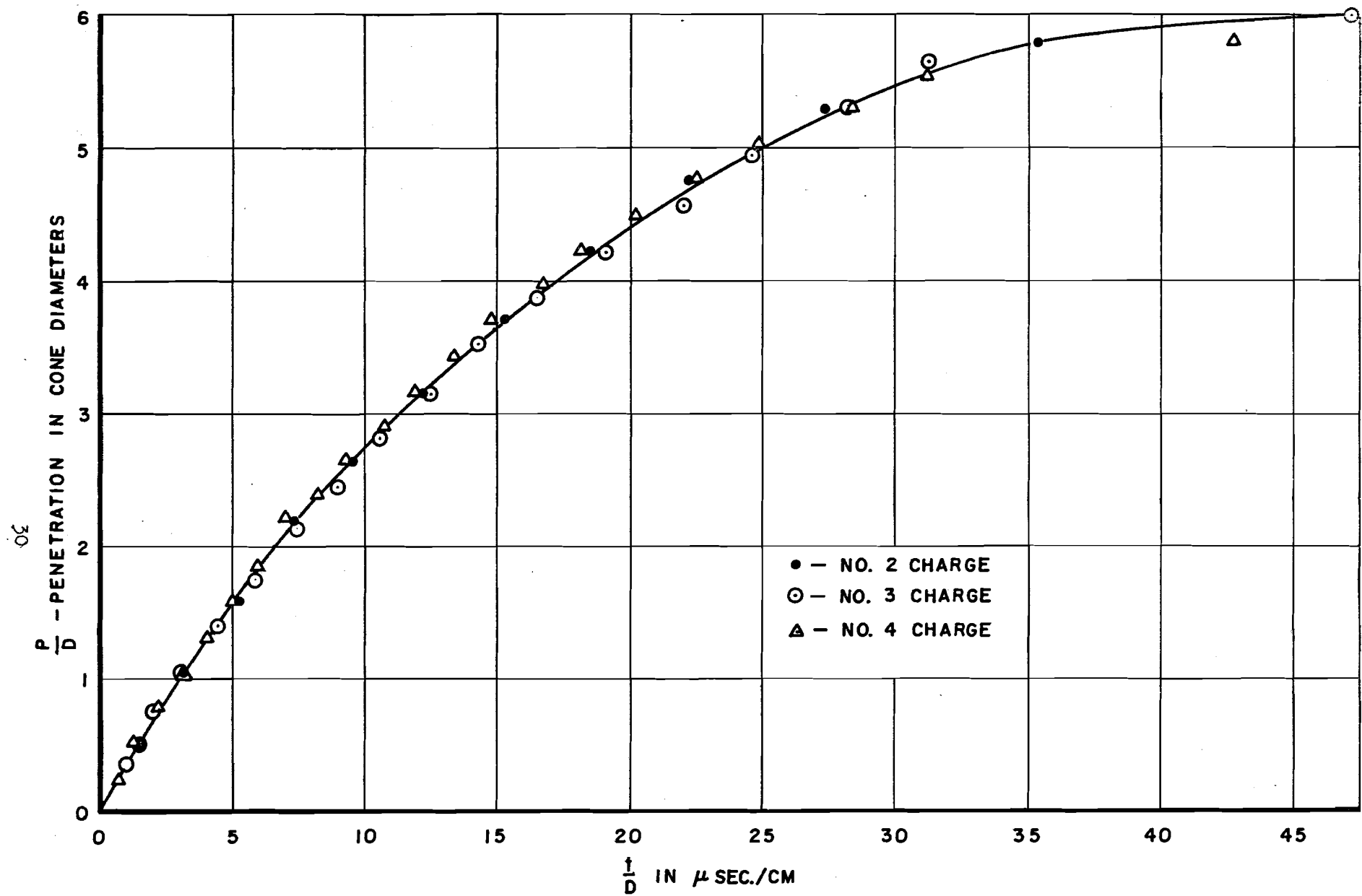Fig. 6. Jet particle number from front vs. cone element position.
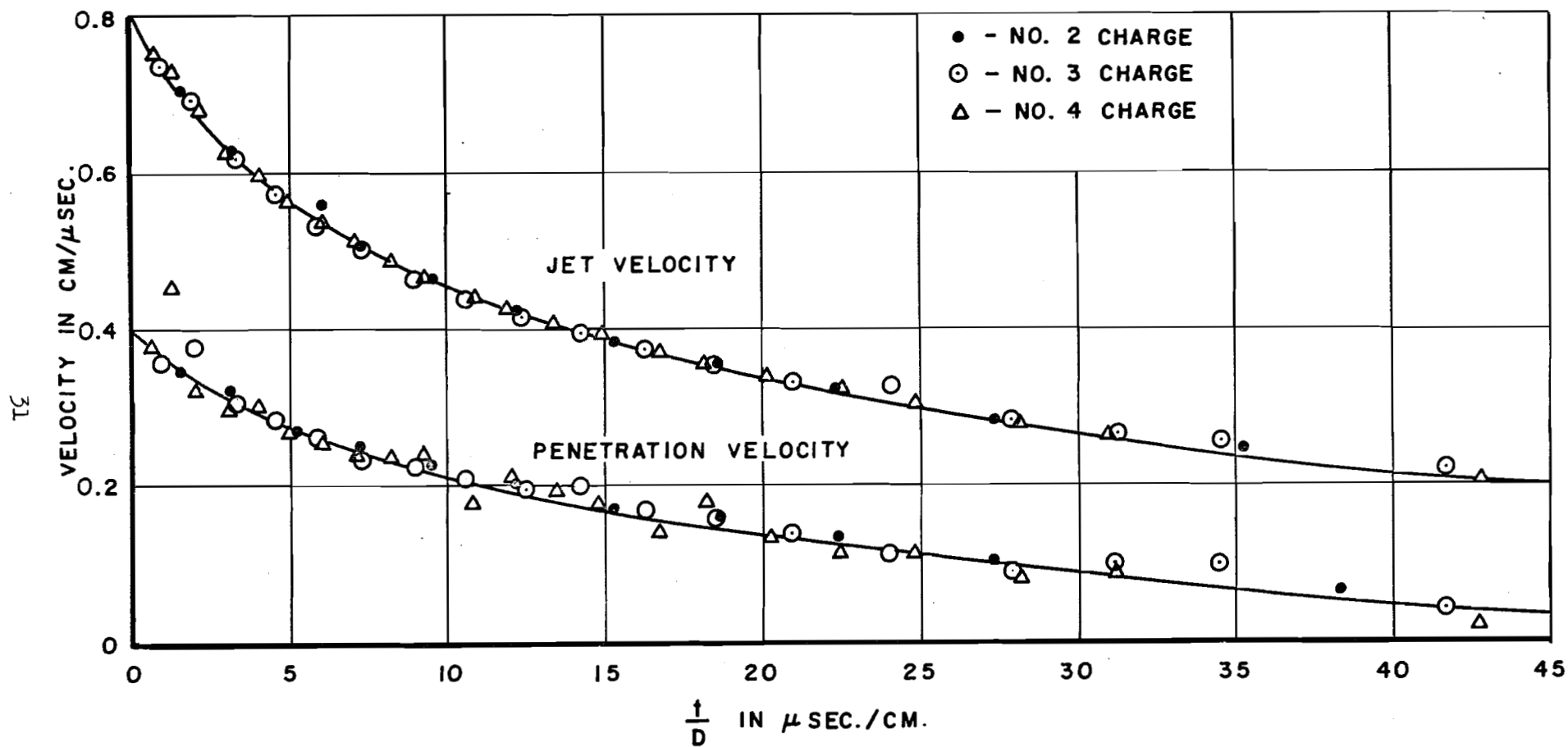
Fig. 7. Target penetration vs. time.
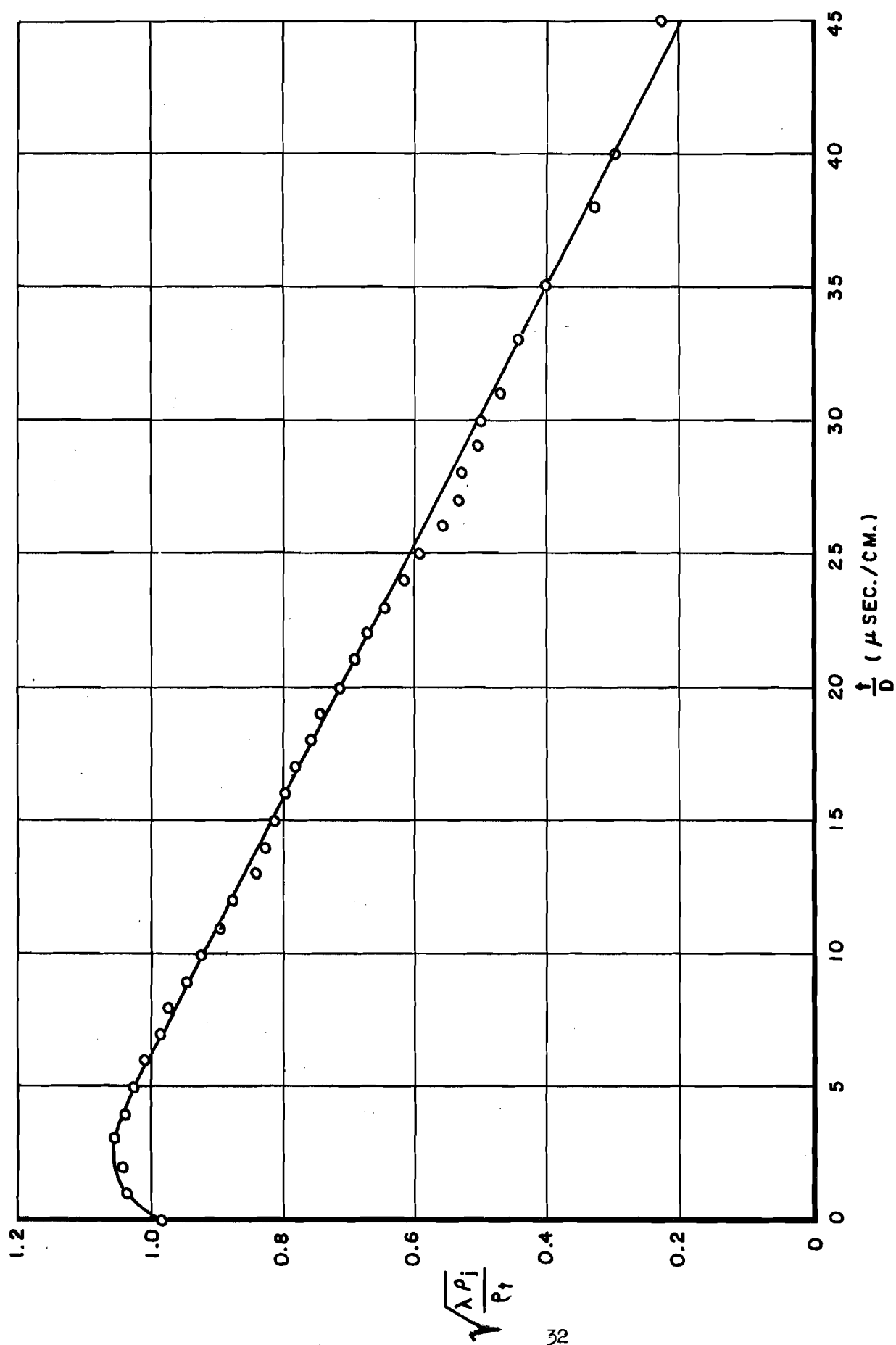
Fig. 8. Penetration and jet velocity vs. time.

31

Fig. 9. "Breakup" factor vs. time after penetration.

$$\sqrt{\frac{\lambda \rho_i}{\rho_t}}$$

32

DISTRIBUTION LIST

| No. of Copies | Organization | No. of Copies | Organization |
|---|---|---|---|
| 4 | Chief of Ordnance<br>Department of the Army<br>Washington 25, D.C.<br>Attn: ORDTB - Bal Sec<br>ORDTU<br>ORDTW | 1 | Commander<br>U.S. Naval Ordnance Test Station<br>China Lake, California<br>Attn: Technical Library |
| 1 | Commanding Officer<br>Diamond Ordnance Fuze Laboratories<br>Washington 25, D.C.<br>Attn: ORDTL - 012 | 1 | Commander<br>U.S. Naval Weapons Laboratory<br>Dahlgren, Virginia |
| 1 | Commanding Officer<br>Diamond Ordnance Fuze Laboratories<br>Washington 25, D.C. | 1 | Director<br>Marine Corps Landing Force<br>Development Center<br>Marine Corps School<br>Quantico, Virginia |
| 10 | Commander<br>Armed Services Technical<br>Information Agency<br>Arlington Hall Station<br>Arlington 12, Virginia<br>Attn: TIPCR | 1 | Commander<br>Air Research and Development<br>Command<br>Andrews Air Force Base<br>Washington 25, D.C.<br>Attn: RDRR2 |
| 10 | Commander<br>British Army Staff<br>British Defence Staff (W)<br>3100 Massachusetts Avenue, N.W.<br>Washington 8, D.C.<br>Attn: Reports Officer | 1 | U.S. Atomic Energy Commission<br>Washington 25, D.C.<br>Attn: Technical Reports Library,<br>Mrs. J. O'Leary for Division<br>of Military Application |
| 4 | Canadian Army Staff<br>2450 Massachusetts Avenue<br>Washington 8, D.C. | 1 | Commanding General<br>U.S. Continental Army Command<br>Fort Monroe, Virginia |
| 3 | Chief, Bureau of Naval Weapons<br>Department of the Navy<br>Washington 25, D.C.<br>Attn: DIS-33 | 1 | President<br>U.S. Army Artillery Board<br>Fort Sill, Oklahoma |
| 2 | Commander<br>Naval Ordnance Laboratory<br>White Oak, Silver Spring 19<br>Maryland | 1 | President<br>U.S. Army Armor Board<br>Fort Knox, Kentucky<br>Attn: Chief, Combat Vehicle<br>Section |
|  |  | 1 | President<br>U.S. Army Infantry Board<br>Fort Benning, Georgia |

DISTRIBUTION LIST

| No. of Copies | Organization | No. of Copies | Organization |
|---|---|---|---|
| 1 | Commandant<br>The Armored School<br>Fort Knox, Kentucky<br>Attn: Combat Development Group<br>Weapons Department | 1 | Commanding Officer<br>Springfield Armory<br>Springfield 1, Massachusetts<br>Attn: Res. 4, Div - TIV |
| 1 | Commandant<br>The Infantry School<br>Fort Benning, Georgia<br>Attn: Combat Developments | 2 | Commanding General<br>Ordnance Ammunition Command<br>Joliet, Illinois<br>Attn: ORDLY - AR-V<br>ORDLY-AR-AR |
| 1 | Commanding Officer<br>Detroit Arsenal<br>28251 Van Dyke Avenue<br>Centerline, Michigan | 1 | Commanding General<br>Ordnance Weapons Command<br>Rock Island, Illinois<br>Attn: Research Branch |
| 2 | Commanding General<br>Frankford Arsenal<br>Philadelphia 37, Pennsylvania<br>Attn: Library Branch, 0270,<br>Bldg. 40 | 1 | Commanding Officer<br>Office of Ordnance Research<br>Box CM, Duke Station<br>Durham, North Carolina |
| 3 | Commanding Officer<br>Picatinny Arsenal<br>Dover, New Jersey<br>Attn: Feltman Research and<br>Engineering Laboratories | 1 | Commanding Officer<br>U.S. Army Combat Development<br>Experimentation Center<br>Fort Ord, California |
| 1 | Commanding Officer<br>Rock Island Arsenal<br>Rock Island, Illinois | 1 | Army Research Office<br>Arlington Hall Station<br>Arlington, Virginia |
| 1 | Commanding Officer<br>Watertown Arsenal<br>Watertown 72, Massachusetts<br>Attn: W.A. Laboratory | 1 | U.S. Department of the Interior<br>Bureau of Mines<br>4800 Forbes Street<br>Pittsburgh 13, Pennsylvania<br>Attn: Chief, Explosive and<br>Physical Sciences<br>Division |
| 1 | Commanding Officer<br>Watervliet Arsenal<br>Watervliet, New York<br>Attn: Mr. A. Muzicka | 1 | Library of Congress<br>Technical Information Division<br>Reference Department<br>Washington 25, D.C.<br>Attn: Bibliograph Section |
| 1 | Commanding General<br>Army Rocket and Guided Missile<br>Agency<br>Redstone Arsenal, Alabama<br>Attn: Technical Library, ORDXR-OTL | | |

34

DISTRIBUTION LIST

| No. of Copies | Organization |
|---|---|
| 1 | Chief of Research and Development<br>Department of the Army<br>Washington 25, D.C.<br>Attn:  Director of Developments<br>        Combat Material Division |
| 1 | Director of Defense Research and<br>    Engineering (OSD)<br>Washington 25, D.C.<br>Attn:  Director/Ordnance |
| 1 | Firestone Tire and Rubber Company<br>Akron 17, Ohio<br>Attn:  Librarian<br>        Mr. C.M. Cox<br>        Defense Research Division |
| 1 | Carnegie Institute of Technology<br>Department of Physics<br>Pittsburgh 13, Pennsylvania<br>Attn:  Professor Emerson M. Pugh |